Ligand field states control photocatalytic efficiency of transition metal oxides

Michael Sachs,[1,2,3]* Liam Harnett-Caulfield,[4] Ernest Pastor,[5,6]* Bernadette Davies,[1] Daniel J. C. Sowood,[1] Benjamin Moss,[1] Andreas Kafizas,[1] Jenny Nelson,[2] Aron Walsh,[4]* James R. Durrant[1]*

[1] Department of Chemistry and Centre for Processable Electronics, Imperial College London, London, U.K.

[2] Department of Physics and Centre for Processable Electronics, Imperial College London, London, U.K.

[3] PULSE Institute for Ultrafast Energy Science, Stanford University, Menlo Park, CA, USA.

[4] Department of Materials and Centre for Processable Electronics, Imperial College London, London, U.K.

[5] CNRS, Univ Rennes, IPR (Institut de Physique de Rennes) - UMR 6251, Rennes, France.

[6] CNRS, Univ Rennes, DYNACOM (Dynamical Control of Materials Laboratory) - IRL2015, The University of Tokyo, Tokyo, Japan.

*email: sachsm@stanford.edu, ernest.pastor@univ-rennes.fr, a.walsh@imperial.ac.uk, j.durrant@imperial.ac.uk

Efficient charge extraction in solar energy conversion devices requires materials that are capable of generating long-lived charge carriers. However, carrier lifetimes vary by orders of magnitude between photoabsorbers and there is no blueprint for the targeted design of materials with intrinsically long lifetimes. Here, we establish a fundamental link between the carrier lifetime and the electronic configuration of transition metal oxides (TMOs). By comparing their deactivation pathways across a range of electronic configurations, we identify a sub-ps relaxation mechanism via metal-centred ligand field (LF) states. These LF states open localised recombination channels that compromise charge and quantum yields in open d-shell TMOs (e.g., Fe_2O_3, Co_3O_4, Cr_2O_3, NiO), which is more reminiscent of molecular complexes than crystalline semiconductors. In contrast, in TMOs with d^0 or d^{10} electronic configurations (e.g., TiO_2, $BiVO_4$), the absence of LF states enables larger yields of long-lived charges and thus more efficient photocatalysis. Notably, our results suggest that charge localisation in the form of polarons can mitigate rapid LF deactivation. These trends translate to other metal-containing semiconductors and open a new pathway to design absorbers with well-controlled non-radiative recombination channels for applications including photovoltaics, photocatalysis, and communication devices.

Photosynthetic devices need to couple short-lived excited states to kinetically slow chemical reactions at the catalyst surface, which requires the generation of long-lived charge carriers.[1] For example, biological photosynthesis sacrifices up to half of its light energy input to gain the carrier lifetimes required to drive chemical reactions.[2] Similarly, lifetime gain via suppression of fast recombination pathways is essential in artificial photosynthetic systems. This suppression is typically achieved through the application of external electrical bias,[3,4] the use of sacrificial reagents,[5] or the construction of rectifying junctions.[6] The design of materials with long intrinsic carrier lifetimes is key for the development of more efficient solar energy conversion devices, however, it remains challenging to develop descriptors capable of predicting carrier lifetimes.

Transition metal oxides (TMOs) are the most widely studied photocatalytic materials,[7] and are of interest for low-cost photovoltaics.[8] Empirically, it has been found that photoexcitation of TMOs with open (d^0) or closed (d^{10}) d-shells can generate long-lived charge carriers with high solar-to-chemical conversion

efficiencies.[9–11] For example, d^0 oxides such as TiO_2 and $SrTiO_3$ have reached quantum efficiencies near unity in photocatalytic applications,[10,12,13] correlated with longer carrier lifetimes. However, light absorption by most d^0 or d^{10} TMOs is limited to the UV region of the solar spectrum, which constrains the amount of useable solar irradiation.

Conversely, open d-shell (d^1-d^9) TMOs absorb more visible light but struggle to efficiently convert their absorbed photons into long-lived charges. For example, α-Fe_2O_3 (d^5) has reached only 34% of its maximum water oxidation photocurrent,[14] despite intense research. The reason for this lower yield of long-lived reactive charges in open d-shell TMOs has remained unclear, raising the question of whether it is possible to synthesise a material with both broad spectral light absorption and high photocatalytic quantum yields over extended parts of the visible range – a combination considered essential for the successful commercialisation of direct solar-to-fuel devices.[15]

Here we use time-resolved optical spectroscopy and electronic structure calculations to establish a correlation between the electronic configuration of the metal atoms in TMO photocatalysts and the attainable carrier lifetime. We find that ligand field (LF) states, resulting from the rearrangement of the electron occupancy within the metal *d* orbitals upon photoexcitation, are responsible for a fast deactivation mechanism that ultimately sets the threshold for the attainable carrier lifetime in open d-shell TMOs. LF states strongly depend on the metal charge state and coordination environment, and have been studied extensively for molecular complexes.[16,17] In contrast, LF states have largely been overlooked in solid state photocatalysts.

Our results suggest that the availability of LF states is responsible for the performance trends observed between open and empty/closed d-shell TMO photocatalysts. Moreover, we find the absence of LF states also explains the success of high-absorbing, high-performing photovoltaic systems such as chalcopyrites (e.g. $CuInSe_2$) and halide perovskites (e.g. $CsPbI_3$). The model we present points towards strong parallels between TMOs and molecules and provides a descriptor to predict and, potentially, extend carrier lifetimes in solar energy conversion materials.

Electronic states in transition metal oxides

To evaluate links between electronic structure and carrier lifetime, we first focus on the optical response of open d-shell oxides in the UV-visible range, as exemplified by Fe_2O_3, Cr_2O_3, and Co_3O_4. The synthesis of the oxides studied herein is described in Supplementary Information section 1 and their structural characterization is shown in Supplementary Information sections 3-4. The distinct absorption features in these materials (**Fig. 1a**) can be understood as follows, with the vertical red line indicating the bandgap (determined via Tauc plots in Supplementary Information section 5). Charge transfer (CT) transitions are optically bright with high oscillator strengths and occur from oxygen to metal (ligand-to-metal, LMCT) or between two metal centres (metal-to-metal, MMCT). Photoexcitation of these transitions leads directly to a degree of spatial charge separation. In contrast, ligand field (LF) transitions are associated with a rearrangement of electron density within the d-orbital manifold on the same metal centre.

Cr_2O_3 has a series of LF transitions at sub-bandgap energies due to the d^3 configuration of Cr(III), which allow the absorption of visible light despite its large bandgap. The transitions around 2.1 eV (590 nm) correspond to spin-allowed $t_{2g}^{\uparrow\uparrow\uparrow}$ to $t_{2g}^{\uparrow\uparrow}e_g^{\uparrow}$ excitations on the Cr(III) ion in an approximately octahedral ligand field[18] and contribute to the green colour of the bulk material. In contrast, sub-bandgap LF transitions in Fe_2O_3, where Fe(III) features a d^5 configuration and exists within an octahedral ligand field,

are spin-forbidden due to the half-filled $t_{2g}^3 e_g^2$ ground state of Fe. These transitions are not well-resolved due to their low oscillator strength, but can be observed from 1.4 eV (886 nm) in bulk samples.[19] Co_3O_4 has CT transitions in our 0.8 – 2.8 eV absorption probe range, plus a combination of long-wavelength LF transitions involving tetrahedral Co(II) d^7 and octahedral Co(III) d^6 ions in the near-infrared range.[20]

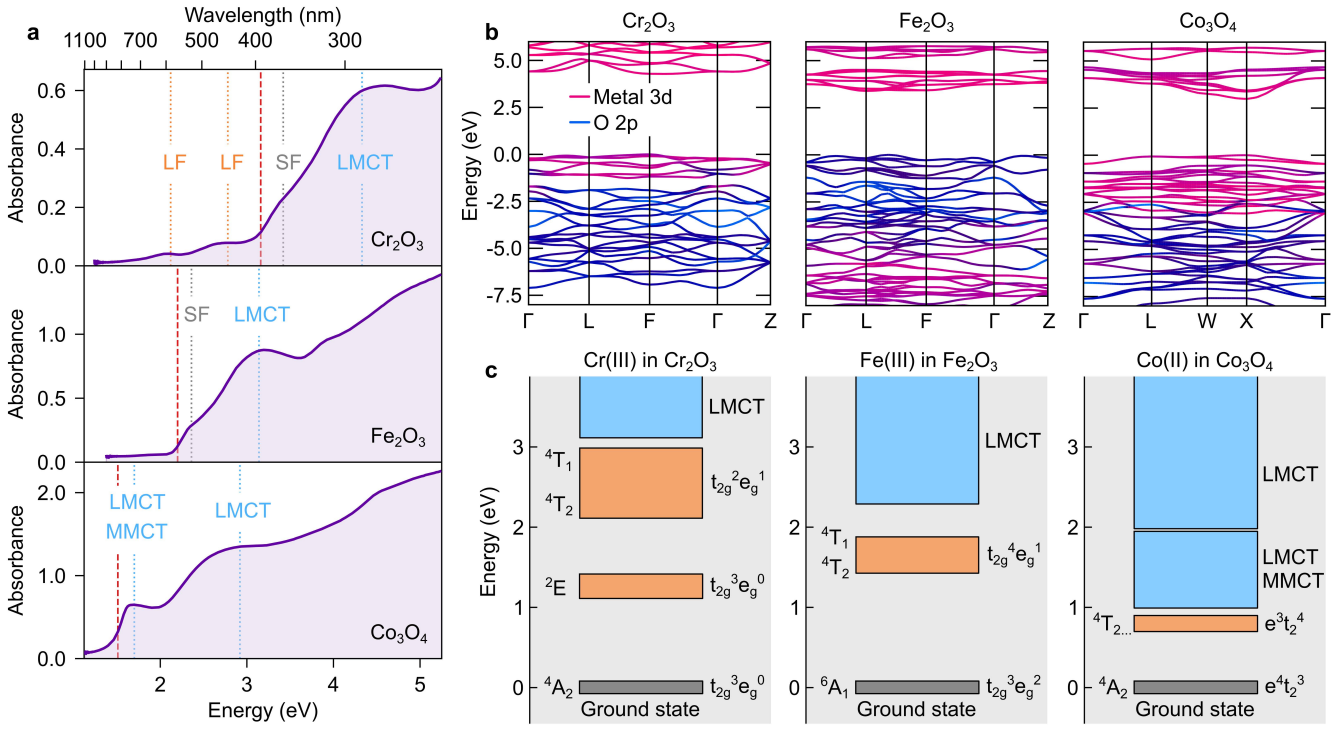

Fig. 1 | Optical and electronic properties of the open d-shell TMOs Cr_2O_3, Fe_2O_3, and Co_3O_4. (**a**) Ground state optical absorption spectra in polycrystalline thin films. The dotted lines indicate ligand field (LF), spin-flip (SF), ligand-to-metal charge transfer (LMCT) and metal-to-metal charge transfer (MMCT) transitions. Herein, we focus on LF and LMCT states. Red dashed lines represent bandgap energies determined by Tauc plots. (**b**) Single-particle electronic band structures calculated from DFT with the HSE06 exchange-correlation functional. (**c**) Electronic state diagrams illustrating that LF excitations lie within the band gap of open d-shell TMOs, opening up pathways for energetic relaxation. The indicative optical transition energies are adapted from References [18], [19], and [21].

The electronic composition of band states is typically rationalised using density functional theory (DFT) calculations as shown in **Fig. 1b**. For our open d-shell TMOs, O *2p* and metal *3d* orbitals dominate the bandgap region of the density of states. While the conduction band edge is predominantly composed of metal *3d* states in all cases, the valence band edge exhibits increasing *O 2p* character from Co_3O_4 to Cr_2O_3 to Fe_2O_3. For comparison, for the empty d-shell TMO TiO_2, the valence band edge consists almost exclusively of O *2p* states.[22] While such orbital pictures provide insights into the charge transfer character of a transition, they do not capture LF excitations.

LF transitions require explicit consideration of excited states that include strong excitonic effects due to their localised nature. The energetics of atomic and molecular excitations are commonly described in state pictures which quantify changes in energy of the entire system, in contrast to changes in orbital or band occupancy. The corresponding LF transitions can be calculated from Tanabe–Sugano diagrams. For example, the tetrahedral Co(II) ion in Co_3O_4 has a $^4A_2$ ground state and a low energy $^4T_2$ excited state, which corresponds to a change in the local electronic configuration from $e^{\uparrow\downarrow\uparrow}t_2^{\uparrow\uparrow\uparrow}$ to $e^{\uparrow\downarrow\uparrow}t_2^{\uparrow\uparrow\uparrow\downarrow}$.[21]

Considering these open d-shell TMOs, each of the transition metals has LF states that lie at energies between the ground state and LMCT excited state (i.e., at sub-bandgap energies) (**Fig. 1c**).[23] Importantly, such LF states are absent for d^0/d^{10} oxides because their empty/filled d-orbitals prevent on-site metal excitations. LF states are intrinsic states because they are a direct consequence of a material's electronic structure, in contrast to other intragap states such as those arising from native defects and impurities. As we explore in the following section, the presence of LF states opens up intrinsic carrier relaxation and recombination pathways, making them a key factor in solar energy conversion devices.

Distinguishing active from inactive charges

To identify the nature of the photoexcited states in our TMOs, we first evaluate the femtosecond – nanosecond transient absorption spectra obtained upon LMCT excitation (**Fig. 2a-c**). These transient spectra consist of two signals with partial overlap: (i) a short-lived broad component observed at sub-bandgap energies, illustrated in yellow as the absorption difference between 0.5 and 1.0 ps, and (ii) a long-lived structured component observed in spectral regions with ground state absorbance, illustrated in purple as the remaining signal after 5.7 ns. The broad component decays on the fs – ps timescale and is most clearly observed at NIR probe energies where its overlap with the structured component is minimised, whereas the structured component has a lifetime of at least nanoseconds. As a result, the structured signal defines the overall spectral shape while the spectral evolution arises mainly from the decay of the broad component.

The broad and positive signal observed at sub-bandgap energies (yellow) is associated with a photoinduced optical absorption, which we assign to active charges that ultimately drive photocatalytic target reactions.[3] Such broad spectral signatures, often accompanied by Drude-like free carrier absorption in the IR range, have been observed in several d^0 TMOs.[24–27] To further corroborate this assignment for open d-shell materials, we take advantage of the isolated LF transitions in Cr_2O_3 which generate spatially localised rather than mobile charges. **Fig. 2d** demonstrates that the broad component is completely absent upon 2.7 eV (460 nm) sub-bandgap LF excitation, suggesting that no mobile charges are generated, and only the more long-lived structured component remains. Conversely, varying the excess energy of mobile charges by changing the excitation energy to different above-bandgap transitions in Co_3O_4 gives rise to essentially the same transient features as LMCT bandgap excitation (Supplementary Fig. 18). We thus conclude that this broad, rapidly decaying spectral feature (shaded in yellow) arises from free carriers in delocalised band-like states as schematically shown in **Fig. 2e**.

We attribute the structured component (purple), observed at or near ground state absorption features, to charges trapped at defect sites. Consistent with this assignment, the amplitude of this structured signal can be modulated via the occupation of sub-bandgap oxygen vacancy states in Fe_2O_3[3,28,29] and $BiVO_4$,[30] up to its complete absence in low-defect monocrystalline Fe_2O_3 films.[31] This structured signal persists up to milliseconds and follows a power law decay at these longer times (Supplementary Fig. 19), which is indicative of a trap-mediated recombination process.[32] More specifically, this signal has previously been assigned to deeply trapped minority carriers that are largely photocatalytically inactive.[28]

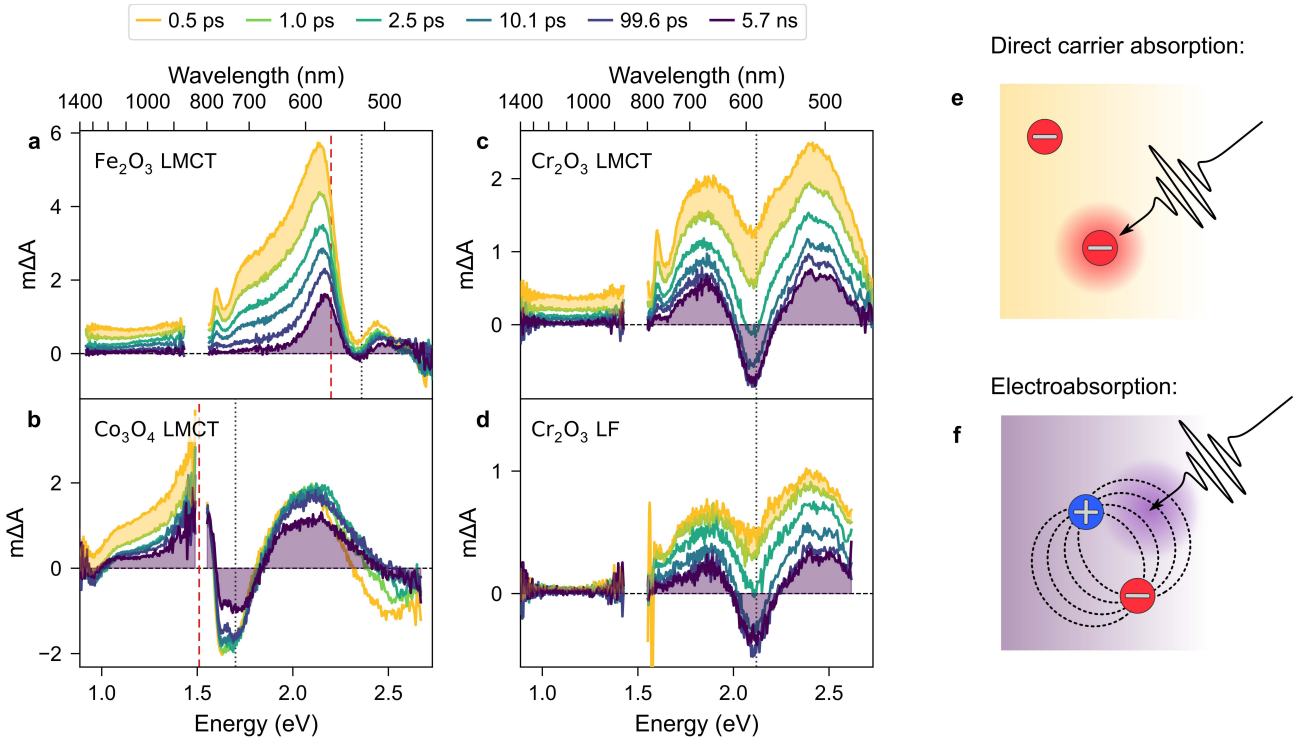

Fig. 2 | Spectral signatures of photogenerated charges on the fs – ns timescale. (a-c) Transient absorption spectra for (**a**) Fe_2O_3, (**b**) Co_3O_4, (**c**) Cr_2O_3 upon LMCT excitation (3.10 eV, 1.68 eV, and 3.40 eV, respectively). (**d**) Transient absorption spectra for Cr_2O_3 upon LF excitation (2.7 eV). Black dashed and red dashed lines indicate the transitions and bandgaps shown in **Fig. 1a**, respectively. The filled yellow and purple regions illustrate the shape of the broad and structured components discussed in the text, originating from **(e)** direct carrier absorption and **(f)** electroabsorption processes, respectively. Note that the same number of photons absorbed were used for comparing LF and LMCT in Cr_2O_3. Any smaller sharp signals observed around 1.6 eV are probe light artefacts rather than real features.

The 2nd derivative-like shape of this structured component (Supplementary Fig. 20) suggests that it results from a broadening of the ground-state optical resonances upon photoexcitation, as exemplified by bleaches at the transition energies (dotted lines) identified in **Fig. 1a**. Transition broadening has been attributed to a Stark effect, caused by local internal electric fields that arise from trapped charges (**Fig. 2f**).[27,30] Such second derivative transient signals have been linked to trapped charges in transition metal selenides[33,34] and halide perovskites,[35,36] as well as to other forms of localised carriers.[37] We explore these less functionally relevant trapped carriers in Supplementary Information section 6, shifting our focus to the more mobile and reactive charges for the remainder of this manuscript.

Metal electronic configuration controls yield of reactive charges

To capture the temporal evolution of reactive charge populations, we turn to the kinetics of the broad component in our transient signal, assigned to carriers in band-like states as detailed above. **Fig. 3** shows transient kinetics probed at sub-bandgap energies for a range of different fluences, representing decays at different charge carrier densities, calculated from a material's absorbance at the used excitation energy and the film thickness. For better comparison, all traces were normalised via division by the carrier density. As a result, overlapping traces reveal charge density-independent (i.e., monomolecular)

processes. In contrast, a divergence between traces suggests a charge density dependent process involving more than one charge, a common example of which is bimolecular electron-hole recombination.

The Co_3O_4 kinetics shown in **Fig. 3a** exhibit two charge carrier density independent kinetic processes, namely a rapid exponential decay with a time constant of 400 fs and a small slowly decaying background. While the slowly decaying background matches the structured component originating from trapped charges, the sub-ps decay is associated with the disappearance of the broad component, suggesting a rapid monomolecular decay of reactive charges, almost irrespective of the charge carrier density studied. However, for Cr_2O_3 (**Fig. 3b**) and Fe_2O_3 (**Fig. 3c**), in addition to this sub-ps decay, we see a broad charge-density-dependent component that decays largely on the ps - ns timescale. The decay of this second population accelerates with increasing charge density, which is indicative of the bimolecular recombination of separated electrons and holes and is consistent with our assignment of this spectral feature to mobile, reactive charges. For comparison, $BiVO_4$, a d^0 metal oxide, primarily exhibits bimolecular recombination kinetics (**Fig. 3d**).

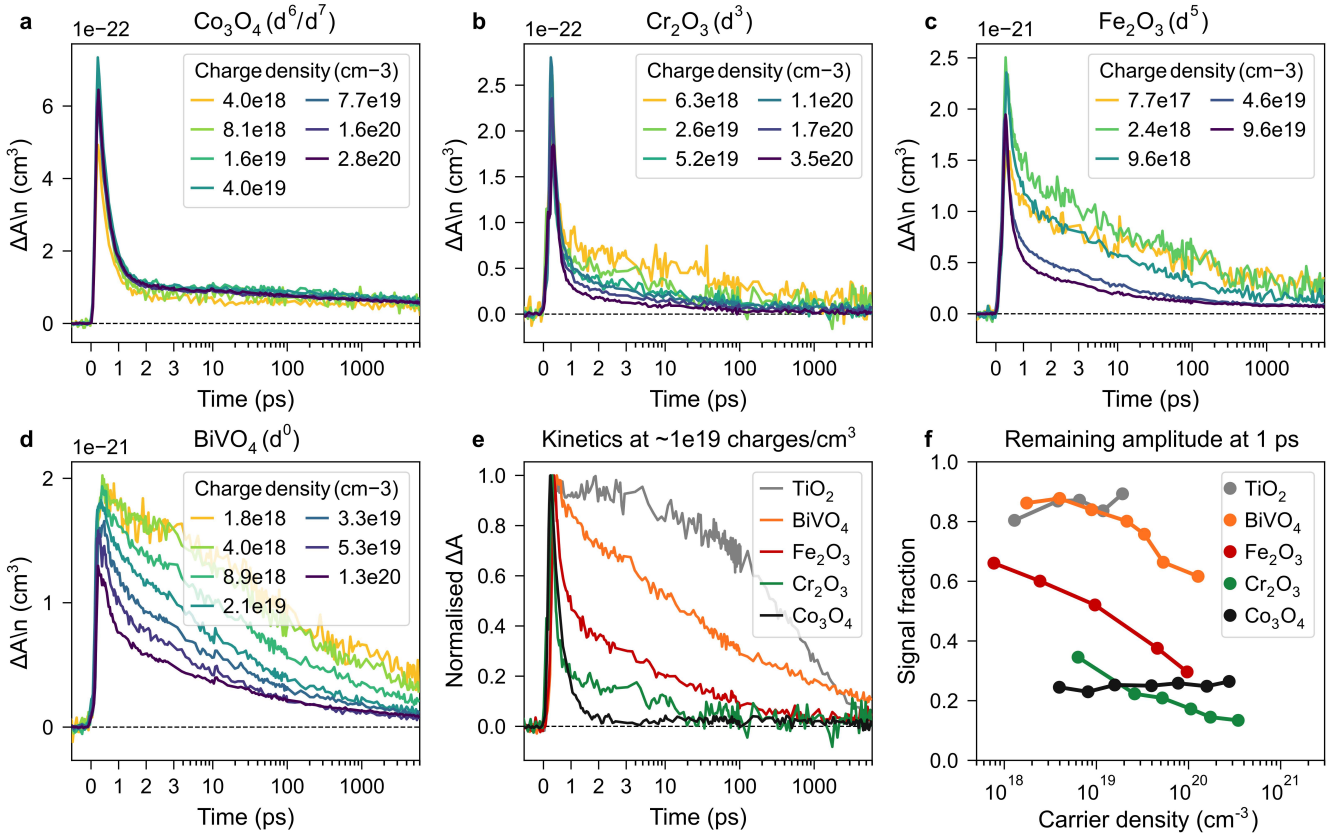

Fig. 3 | Dynamics of photogenerated charges on the fs – ns timescale. (a-d) Transient absorption kinetics probed at 1.13 eV (1100 nm) as a function of photogenerated carrier density for (**a**) Co_3O_4 (1.68 eV excitation), (**b**) Cr_2O_3 (3.40 eV excitation), (**c**) Fe_2O_3 (3.10 eV excitation), (**d**) $BiVO_4$ (3.68 eV excitation). All traces were divided by the photogenerated carrier density to more easily distinguish between monomolecular and bimolecular recombination processes. (**e**) Comparison of the broad component kinetics seen in Co_3O_4, Cr_2O_3, Fe_2O_3 and $BiVO_4$ obtained from low fluence measurements (1e19 charges/cm^3), where any slowly decaying background arising from a structured component has been subtracted. Analogous kinetics for TiO_2 are included for comparison (see also Ref. [38]). Traces have been normalised to the signal maximum. (**f**) Remaining signal fraction at 1 ps as a function of carrier density, illustrating a rapid sub-ps decay in open d-shell TMOs.

It is apparent that the lifetime of photogenerated charges strongly varies between oxides. **Fig. 3e** compares the kinetics of reactive charges seen at low fluences in **Fig. 3a-c** across oxides, for which we subtract the structured component (Supplementary Fig. 23). The sub-ps monomolecular decay is observed for all our open d-shell oxides, which we attribute to a loss of reactive charges via relaxation through their LF states, illustrated in **Fig. 1c**. This LF relaxation process is temperature-independent and thus barrierless (Supplementary Fig. 22). In d^0 and d^{10} TMOs, where LF states are absent, this relaxation pathway is suppressed and charges undergo slower bimolecular recombination, as illustrated for $BiVO_4$ and TiO_2 anatase.[38] As a result, a substantially larger proportion of the signal decays within the first picosecond in open d-shell TMOs compared to those with d^0 configurations (**Fig. 3f**).

Furthermore, our data suggest that differences in energy and spin between the LMCT and LF states in open d-shell TMOs control the dominance of LF relaxation. The dynamics of Co_3O_4 are strongly dominated by LF relaxation, in line with a small LMCT-LF energy gap and a spin-allowed LMCT-LF transition. In contrast, Fe_2O_3 exhibits a larger population of longer-lived, reactive charges than the other open d-shell metal oxides, which can be attributed to its LMCT-LF transition being spin forbidden, or to lower electron-phonon coupling (Supplementary Information section 5).

Correlating electronic configuration and carrier lifetime

We now extend our observations to a wider range of TMOs. We first consider the effects of bandgap size and doping density on carrier lifetime. In NiO, Ni(II) has a d^8 configuration with lower energy LF transitions at 1.1, 1.8 and 3.2 eV.[23] For an open d-shell TMO, NiO has a large bandgap of ca. 3.8 eV yet exhibits fast monomolecular recombination (Supplementary Fig. 24), demonstrating that it is not the typically smaller bandgap of open d-shell TMOs that causes higher recombination rates as might have been expected based on the energy gap law.[39]

Conversely, CdO is a closed d-shell d^{10} TMO with an optical bandgap similar to Fe_2O_3, yet exhibits long-lived mobile charges (Supplementary Fig. 25). Mobile charges in d^{10} TMOs appear in the form of a near-band edge bleach, similar to widely used photovoltaic materials such as lead halide perovskites[40] or $Cu(In,Ga)Se_2$,[41] which incorporate Pb(II) and Cu(I) d^{10} metal centres, respectively. At the other end of the periodic table, d^0 oxides such as $BiVO_4$ and anatase TiO_2 exhibit bimolecular behaviour, and exhibit slower decays than open d-shell oxides even in materials with large intrinsic doping densities (rutile TiO_2, WO_3).[38,42]

In open d-shells TMOs, d-states incorporate into the valence band and/or introduce lower energy LF transitions, giving rise to more extended visible light absorption, whereas TMOs with d^0 or d^{10} configurations tend to absorb a relatively small fraction of solar photons due to their larger bandgaps (**Fig. 4a**). At the same time, the availability of LF states associated with partially occupied d-orbitals induces a pathway for rapid relaxation of LMCT states, leading to much shorter overall lifetimes of reactive charges (**Fig. 4b**). Interestingly, certain d^{10} materials, including CdO and the lead halide perovskite (MAPI) and chalcogenide (CIGSe) semiconductors primarily used in solar cells, break this anticorrelation and offer both extended light absorption and long carrier lifetimes.

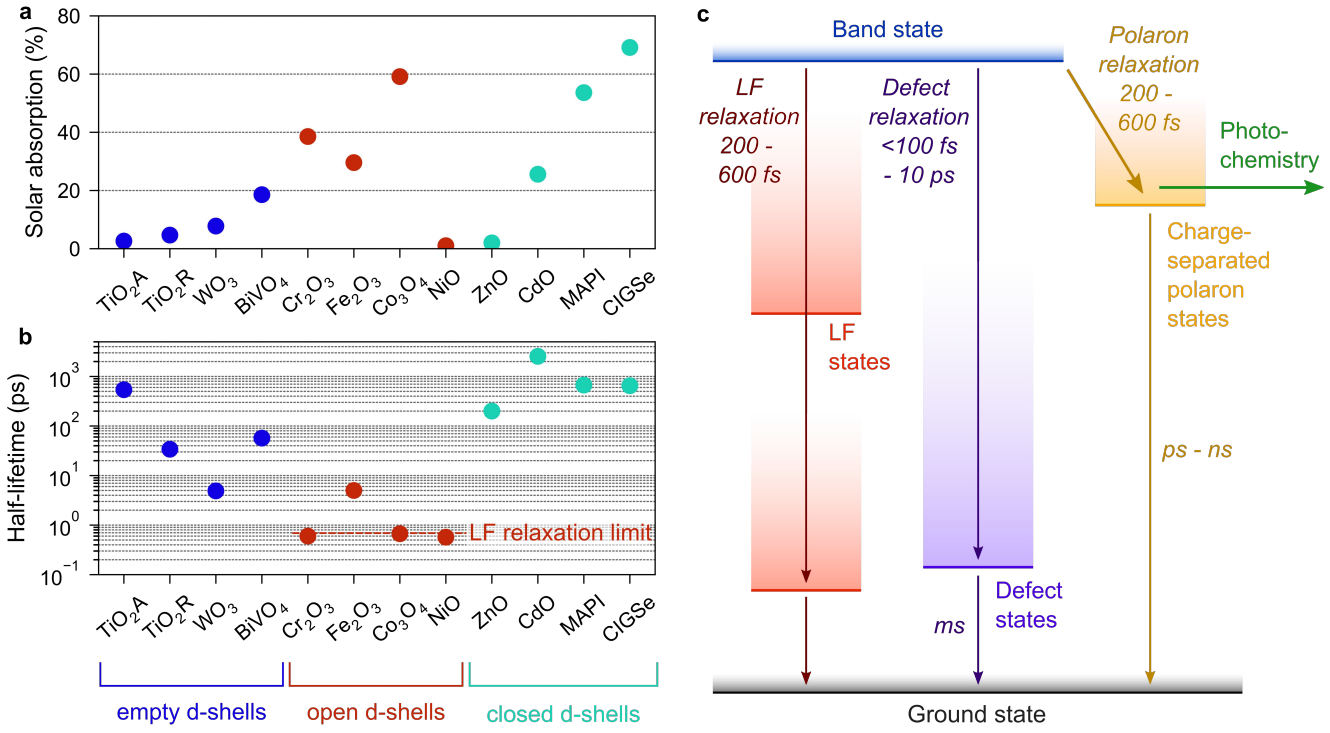

Fig. 4 | Effect of electronic configuration on light absorption and carrier lifetime. (**a**) Light harvesting potential in various transition-metal-containing light absorbers measured as a percentage of absorbed solar power for an AM 1.5 solar spectrum, assuming full absorption of photons with an energy above the absorption onset. (**b**) Half-lifetime of reactive charges at the lowest used fluence, including literature values for TiO_2,[38] WO_3,[42] ZnO,[43] MAPI,[40] and CIGSe.[41] (**c**) Electronic state diagram summarizing the possible localisation and recombination processes upon photoexcitation.

Competing charge relaxation pathways

Our results point to rapid relaxation through LF states being the primary reason for the insufficient activity of open d-shell photocatalysts – a pathway which has received little attention to date for solid state materials. LF relaxation is non-radiative, consistent with the negligible photoluminescence of open d-shell TMOs, and is most pronounced for spin and parity-allowed transitions (e.g. in Co_3O_4). By combining the findings presented herein with existing literature,[38,40–43] we establish a generalised photophysical model of TMO semiconductors, as illustrated in **Fig. 4c**. Upon bandgap photoexcitation, relatively delocalised but short-lived band states are generated, which subsequently evolve via one of three pathways: (i) LF states promote the sub-ps relaxation of these band-like charges in open d-shell TMOs, (ii) minority carrier trapping occurs in spatial proximity to physical defects, predominantly on the sub-100 fs timescale but extending out to 10 ps for some materials such as $BiVO_4$,[30] (iii) band-like charges localise as spatially separated polarons which subsequently recombine bimolecularly on the ps-ns timescale, and can drive chemical reactions on longer timescales, e.g. in the presence of electrical bias.

An energy cascade is created if the energy gaps between LF states are sufficiently small, supporting fast relaxation through non-radiative dissipation of energy via electron-phonon coupling. The prominence of LF relaxation is a materials property, in line with the associated decay being independent of applied potential[3,44] or defect concentration.[31] LF relaxation is driven by the electronic configuration of the metal

centre, consistent with an analogous fast relaxation pathway being observed for a number of solvated molecules that incorporate open d-shell transition metal centres, where fast intersystem crossing followed by rapid internal conversion through LF states leads to short excited state lifetimes.[45,46] LF relaxation in open d-shell TMOs is also in line with an observed lower yield of mobile carriers in Fe_2O_3 compared to TiO_2,[47] and phenomenologically similar to carrier relaxation though high densities of defect states in defect-rich WO_3.[42]

Polaron formation occurs with a non-radiative energy loss,[48–50] and the resultant lower mobility of polarons compared to more band-like charges is largely considered to be detrimental to electronic device function. However, our data suggests that ultrafast polaron formation also presents a way to combat the rapid LF relaxation in open d-shell TMOs by stabilising a spatial separation of localised charges. Such localisation-induced charge separation has also been suggested to be important in organic solar cells, analogous to Onsager models of auto-ionisation.[51]

A sub-ps formation of small polarons in Fe_2O_3 has been inferred using transient XUV spectroscopy[52–55] and pump-push photocurrent detection,[44] with comparably fast polaron formation dynamics being observed in materials such as α-FeOOH,[56] CeO_2,[57] and NiO.[58] Our observation of LF relaxation on the same timescale suggests a kinetic competition between these processes, meaning that the formation of polarons in open d-shell TMOs is ultimately limited to the sub-ps timescale due to the rapid depletion of band states via LF relaxation. The resulting polaron population defines the number of potentially active charges and is therefore a central descriptor for activity, as supported by studies on n-type TMOs where the application of positive potential slows down[3,59,60] the bimolecular recombination of polarons and gives rise to long-lived reactive holes.

In the presence of structural defects such as oxygen vacancies, carrier localisation can also occur via trapping of minority charges, and if the associated trap states are energetically deep they can render the localised charge inactive (see Supplementary Information section 6). Minority carrier trapping in open d-shell TMOs has been observed to take place mainly from the more delocalised band states on a sub-100 fs timescale,[28] although it can extend out to 10 ps in $BiVO_4$.[30] Once polarons form, their probability of encountering a physical defect over their lifetime decreases due to their more confined wavefunctions, enabling longer polaron diffusion lengths in some cases[61].

Conclusions

In summary, we attribute the prominent sub-ps decay of band charges in open d-shell transitional metal oxides to relaxation through ligand field (LF) states. While optical transitions involving LF states extend the visible light absorption of many oxides, causing coloration, they also result in unavoidable energy losses. These losses lead to carrier deactivation, lowering the yield of reactive charges and thus the attainable quantum yield. In this way, the fate of band charges is determined within the first picosecond after photoexcitation, highlighting the importance of ultrafast processes in the evaluation of photocatalytic performance. Our results suggest that not only band energies, but also the presence and energetics of optically dark LF states, as captured in state pictures, must be considered as key performance descriptors in screening studies of new materials. LF states are insensitive to applied potential, defect concentration, or temperature, suggesting that new strategies will be required for their mitigation.

While the ligand field transitions are largely associated with the identity of the metal, they can in principle be influenced by structural (e.g. octahedral vs tetrahedral environments), mechanical (e.g. increased

ligand field through compressive strain) or chemical (e.g. altering the ligand field strength in oxyhalide and oxypnictide materials) factors that may provide routes to supress their effects. Notably, the trends we observe for metal oxides readily align with high-performance lead halide perovskite and chalcogenide semiconductors, which have largely been applied as photoabsorbers photovoltaics, that are invariably based on d^{10} metals. To achieve higher solar to energy conversion efficiencies, our data highlights a need to further develop d^0 and d^{10} metal oxides, which naturally avoid this ultrafast carrier deactivation due to the absence of LF states, with extended visible light absorption.

Acknowledgements

The authors thank Zhipeng Lin for carrying out Raman measurements under 532 nm excitation, and Shababa Selim for preparing the $BiVO_4$ thin film. M.S. thanks Imperial College for a President's PhD Scholarship and EPSRC for a Doctoral Prize Fellowship. J.R.D. gratefully acknowledges funding from the ERC (AdG 291482 Intersolar). A.K. thanks the EPSRC for a Programme Grant (EP/W017075/1). EP thanks the support of the CNRS and the French Agence Nationale de la Recherche (ANR), under grant ANR-22-CPJ2-0053-01. Funded/Co-funded by the European Union (ERC, PhotoDefect, 101076203). J.N. thanks the European Research Council for award of an Advanced Grant (CAPACITY, no. 7427028) and the Royal Society for award of a Research Professorship. Views and opinions expressed are however those of the authors only and do not necessarily reflect those of the European Union or the European Research Council. Neither the European Union nor the granting authority can be held responsible for them.

Author contributions

M.S., E.P., and J.R.D. designed the experimental protocol. Except for $BiVO_4$, M.S. prepared the metal oxide films. B.D. carried out temperature-dependent ultrafast transient absorption (TA) measurements and analysed the data. D.J.C.S. collected ultrafast TA data on Co_3O_4 at different excitation energies, µs-s TA data on Fe_2O_3 and Co_3O_4, and analysed the data. M.S. performed all other TA measurements, and collected the UV-vis absorption, XRD, and 633 nm Raman data. B.M. carried out the scanning electron microscopy measurements. L.H.-C. performed the band structure calculations. A.K. analysed the XRD data and supervised the XRD and Raman work. M.S. analysed all other data. M.S., E.P, J.N., and J.R.D. discussed and interpreted the experimental results in the context of this paper. J.R.D and E.P. supervised all other experimental work, and A.W. supervised the theory work. M.S., E.P., J.R.D., and A.W. wrote the manuscript with input from all other co-authors.

Data availability

All shown data will be deposited on the open-access repository Zenodo after formal journal acceptance.

Competing interests

The authors declare no competing interests.

References

1. Godin, R., Kafizas, A. & Durrant, J. R. Electron transfer dynamics in fuel producing photosystems. *Curr. Opin. Electrochem.* **2**, 136–143 (2017).
2. Godin, R. & Durrant, J. R. Dynamics of photoconversion processes: the energetic cost of lifetime gain in photosynthetic and photovoltaic systems. *Chem. Soc. Rev.* **50**, 13372–13409 (2021).
3. Pendlebury, S. R. *et al.* Ultrafast Charge Carrier Recombination and Trapping in Hematite Photoanodes under Applied Bias. *J. Am. Chem. Soc.* **136**, 9854–9857 (2014).
4. Cowan, A. J., Tang, J., Leng, W., Durrant, J. R. & Klug, D. R. Water Splitting by Nanocrystalline TiO 2 in a Complete Photoelectrochemical Cell Exhibits Efficiencies Limited by Charge Recombination. *J. Phys. Chem. C* **114**, 4208–4214 (2010).
5. Pellegrin, Y. & Odobel, F. Sacrificial electron donor reagents for solar fuel production. *Comptes Rendus Chim.* **20**, 283–295 (2017).
6. Moniz, S. J. a., Shevlin, S. a., Martin, D. J., Guo, Z.-X. & Tang, J. Visible-light driven heterojunction photocatalysts for water splitting – a critical review. *Energy Env. Sci* **8**, 731–759 (2015).
7. Fujishima, A. & Honda, K. Electrochemical Photolysis of Water at a Semiconductor Electrode. *Nature* **238**, 37–38 (1972).
8. Rühle, S. *et al.* All-Oxide Photovoltaics. *J. Phys. Chem. Lett.* **3**, 3755–3764 (2012).
9. Wang, Q. *et al.* Scalable water splitting on particulate photocatalyst sheets with a solar-to-hydrogen energy conversion efficiency exceeding 1%. *Nat. Mater.* 1–3 (2016) doi:10.1038/nmat4589.
10. Takata, T. *et al.* Photocatalytic water splitting with a quantum efficiency of almost unity. *Nature* **581**, 411–414 (2020).
11. Wang, S. *et al.* New BiVO4 Dual Photoanodes with Enriched Oxygen Vacancies for Efficient Solar-Driven Water Splitting. *Adv. Mater.* **30**, 1800486 (2018).
12. Liu, M., Snapp, N. de L. & Park, H. Water photolysis with a cross-linked titanium dioxide nanowire anode. *Chem. Sci.* **2**, 80–87 (2010).
13. Wilson, A. A. *et al.* Transient absorption spectroscopy reveals that slow bimolecular recombination in SrTiO3 underpins its efficient photocatalytic performance. *Chem. Commun.* (2023) doi:10.1039/D3CC04616H.
14. Kim, J. Y. *et al.* Single-crystalline, wormlike hematite photoanodes for efficient solar water splitting. *Sci. Rep.* **3**, 2681 (2013).
15. Chen, S., Takata, T. & Domen, K. Particulate photocatalysts for overall water splitting. *Nat. Rev. Mater.* **2**, 17050 (2017).
16. Zhang, W. & Gaffney, K. J. Mechanistic Studies of Photoinduced Spin Crossover and Electron Transfer in Inorganic Complexes. *Acc. Chem. Res.* **48**, 1140–1148 (2015).
17. Wegeberg, C. & Wenger, O. S. Luminescent First-Row Transition Metal Complexes. *JACS Au* **1**, 1860–1876 (2021).
18. McClure, D. S. Comparison of the Crystal Fields and Optical Spectra of Cr 2 O 3 and Ruby. *J. Chem. Phys.* **38**, 2289–2294 (1963).

19. Marusak, L. A., Messier, R. & White, W. B. Optical absorption spectrum of hematite, αFe2O3 near IR to UV. *J. Phys. Chem. Solids* **41**, 981–984 (1980).
20. Waegele, M. M., Doan, H. Q. & Cuk, T. Long-Lived Photoexcited Carrier Dynamics of d – d Excitations in Spinel Ordered Co 3 O 4. *J. Phys. Chem. C* **118**, 3426–3432 (2014).
21. Miedzinska, K. M. E., Hollebone, B. R. & Cook, J. G. An assigment of the optical absorption spectrum of mixed valence Co3O4 spinel films. *J. Phys. Chem. Solids* **48**, 649–656 (1987).
22. Scanlon, D. O. *et al.* Band alignment of rutile and anatase TiO2. *Nat. Mater.* **12**, 798–801 (2013).
23. Cox, P. A. *Transition Metal Oxides: An Introduction to Their Electronic Structure and Properties*. (Clarendon Press, 2010).
24. Yoshihara, T. *et al.* Identification of Reactive Species in Photoexcited Nanocrystalline TiO 2 Films by Wide-Wavelength-Range (400−2500 nm) Transient Absorption Spectroscopy. *J. Phys. Chem. B* **108**, 3817–3823 (2004).
25. Yamada, Y., Yasuda, H., Tayagaki, T. & Kanemitsu, Y. Photocarrier recombination dynamics in highly excited SrTiO3 studied by transient absorption and photoluminescence spectroscopy. *Appl. Phys. Lett.* **95**, 121112 (2009).
26. Tamaki, Y., Hara, K., Katoh, R., Tachiya, M. & Furube, A. Femtosecond Visible-to-IR Spectroscopy of TiO2 Nanocrystalline Films: Elucidation of the Electron Mobility before Deep Trapping. *J. Phys. Chem. C* **113**, 11741–11746 (2009).
27. Cooper, J. K. *et al.* Physical Origins of the Transient Absorption Spectra and Dynamics in Thin-Film Semiconductors: The Case of BiVO 4. *J. Phys. Chem. C* **122**, 20642–20652 (2018).
28. Barroso, M., Pendlebury, S. R., Cowan, A. J. & Durrant, J. R. Charge carrier trapping, recombination and transfer in hematite (α-Fe2O3) water splitting photoanodes. *Chem. Sci.* **4**, 2724 (2013).
29. Forster, M. *et al.* Oxygen deficient α-Fe 2 O 3 photoelectrodes: a balance between enhanced electrical properties and trap-mediated losses. *Chem Sci* **6**, 4009–4016 (2015).
30. Selim, S. *et al.* Impact of Oxygen Vacancy Occupancy on Charge Carrier Dynamics in BiVO4 Photoanodes. *J. Am. Chem. Soc.* **141**, 18791–18798 (2019).
31. Fan, Y., Lin, Y., Wang, K., Zhang, K. H. L. & Yang, Y. Intrinsic polaronic photocarrier dynamics in hematite. *Phys. Rev. B* **103**, 085206 (2021).
32. Godin, R., Wang, Y., Zwijnenburg, M. A., Tang, J. & Durrant, J. R. Time-Resolved Spectroscopic Investigation of Charge Trapping in Carbon Nitrides Photocatalysts for Hydrogen Generation. *J. Am. Chem. Soc.* **139**, 5216–5224 (2017).
33. Norris, D. J., Sacra, A., Murray, C. B. & Bawendi, M. G. Measurement of the size dependent hole spectrum in CdSe quantum dots. *Phys. Rev. Lett.* **72**, 2612–2615 (1994).
34. Klimov, V. I. Optical Nonlinearities and Ultrafast Carrier Dynamics in Semiconductor Nanocrystals. *J. Phys. Chem. B* **104**, 6112–6123 (2000).

35. Scholz, M., Flender, O., Oum, K. & Lenzer, T. Pronounced Exciton Dynamics in the Vacancy-Ordered Bismuth Halide Perovskite (CH 3 NH 3) 3 Bi 2 I 9 Observed by Ultrafast UV–vis–NIR Transient Absorption Spectroscopy. *J. Phys. Chem. C* **121**, 12110–12116 (2017).
36. Sadighian, J. C., Wilson, K. S., Crawford, M. L. & Wong, C. Y. Evolving Stark Effect During Growth of Perovskite Nanocrystals Measured Using Transient Absorption. *Front. Chem.* **8**, (2020).
37. Bouduban, M. E. F., Burgos-Caminal, A., Ossola, R., Teuscher, J. & Moser, J.-E. Energy and charge transfer cascade in methylammonium lead bromide perovskite nanoparticle aggregates. *Chem. Sci.* **8**, 4371–4380 (2017).
38. Sachs, M., Pastor, E., Kafizas, A. & Durrant, J. R. Evaluation of Surface State Mediated Charge Recombination in Anatase and Rutile TiO2. *J. Phys. Chem. Lett.* **7**, 3742–3746 (2016).
39. Caspar, J. V., Kober, E. M., Sullivan, B. P. & Meyer, T. J. Application of the energy gap law to the decay of charge-transfer excited states. *J. Am. Chem. Soc.* **104**, 630–632 (1982).
40. Chen, B. A., Pang, G. T., Lan, X. Q., He, Z. B. & Chen, R. Strong band filling induced significant excited state absorption in MAPbI3 under high pump power. *Mater. Today Phys.* **14**, 100228 (2020).
41. Chang, Y.-H. *et al.* Insights from Transient Absorption Spectroscopy into Electron Dynamics Along the Ga-Gradient in Cu(In,Ga)Se2 Solar Cells. *Adv. Energy Mater.* **11**, 2003446 (2021).
42. Sachs, M. *et al.* Effect of oxygen deficiency on the excited state kinetics of WO3 and implications for photocatalysis. *Chem. Sci.* **10**, 5667–5677 (2019).
43. Lettieri, S., Capello, V., Santamaria, L. & Maddalena, P. On quantitative analysis of interband recombination dynamics: Theory and application to bulk ZnO. *Appl. Phys. Lett.* **103**, 241910 (2013).
44. Pastor, E. *et al.* In situ observation of picosecond polaron self-localisation in α-Fe2O3 photoelectrochemical cells. *Nat. Commun.* **10**, 3962 (2019).
45. Gawelda, W. *et al.* Ultrafast Nonadiabatic Dynamics of [FeII(bpy)3]2+ in Solution. *J. Am. Chem. Soc.* **129**, 8199–8206 (2007).
46. Zhang, W. *et al.* Tracking excited-state charge and spin dynamics in iron coordination complexes. *Nature* **509**, 345–348 (2014).
47. Grave, D. A. *et al.* Extraction of mobile charge carrier photogeneration yield spectrum of ultrathin-film metal oxide photoanodes for solar water splitting. *Nat. Mater.* **20**, 833–840 (2021).
48. Lohaus, C., Klein, A. & Jaegermann, W. Limitation of Fermi level shifts by polaron defect states in hematite photoelectrodes. *Nat. Commun.* **9**, 4309 (2018).
49. Pastor, E. *et al.* Electronic defects in metal oxide photocatalysts. *Nat. Rev. Mater.* 1–19 (2022) doi:10.1038/s41578-022-00433-0.
50. Franchini, C., Reticcioli, M., Setvin, M. & Diebold, U. Polarons in materials. *Nat. Rev. Mater.* 1–27 (2021) doi:10.1038/s41578-021-00289-w.

51. Clarke, T. M. & Durrant, J. R. Charge Photogeneration in Organic Solar Cells. *Chem. Rev.* **110**, 6736–6767 (2010).

52. Carneiro, L. M. *et al.* Excitation-wavelength-dependent small polaron trapping of photoexcited carriers in α-Fe2O3. *Nat. Mater.* **16**, 819–825 (2017).

53. Biswas, S., Husek, J., Londo, S. & Baker, L. R. Highly Localized Charge Transfer Excitons in Metal Oxide Semiconductors. *Nano Lett.* **18**, 1228–1233 (2018).

54. Biswas, S., Wallentine, S., Bandaranayake, S. & Baker, L. R. Controlling polaron formation at hematite surfaces by molecular functionalization probed by XUV reflection-absorption spectroscopy. *J. Chem. Phys.* **151**, 104701 (2019).

55. Husek, J., Cirri, A., Biswas, S. & Baker, L. R. Surface electron dynamics in hematite (α-Fe 2 O 3): correlation between ultrafast surface electron trapping and small polaron formation. *Chem. Sci.* **8**, 8170–8178 (2017).

56. Porter, I. J. *et al.* Photoexcited Small Polaron Formation in Goethite (α-FeOOH) Nanorods Probed by Transient Extreme Ultraviolet Spectroscopy. *J. Phys. Chem. Lett.* **9**, 4120–4124 (2018).

57. Pelli Cresi, J. S. *et al.* Ultrafast Formation of Small Polarons and the Optical Gap in CeO2. *J. Phys. Chem. Lett.* **11**, 5686–5691 (2020).

58. Biswas, S., Husek, J., Londo, S. & Baker, L. R. Ultrafast Electron Trapping and Defect-Mediated Recombination in NiO Probed by Femtosecond Extreme Ultraviolet Reflection–Absorption Spectroscopy. *J. Phys. Chem. Lett.* **9**, 5047–5054 (2018).

59. Cowan, A. J., Leng, W., Barnes, P. R. F., Klug, D. R. & Durrant, J. R. Charge carrier separation in nanostructured TiO2 photoelectrodes for water splitting. *Phys. Chem. Chem. Phys.* **15**, 8772 (2013).

60. Ma, Y., Pendlebury, S. R., Reynal, A., Le Formal, F. & Durrant, J. R. Dynamics of photogenerated holes in undoped BiVO 4 photoanodes for solar water oxidation. *Chem Sci* **5**, 2964–2973 (2014).

61. Kay, A. *et al.* Wavelength Dependent Photocurrent of Hematite Photoanodes: Reassessing the Hole Collection Length. *J. Phys. Chem. C* **121**, 28287–28292 (2017).